SYMMETRY OF ILLUMINATION AND IMPLOSION OF HOTRAUM TARGETS FOR HEAVY ION INERTIAL FUSION

M.M. BASKO*
Max-Planck-Institut für Quantenoptik,
Garching, Germany

ABSTRACT. The symmetry of implosion of the hotraum target that has been proposed by J. Meyer-ter-Vehn and the author is analysed in the case when the target is driven by a non-spherical ensemble of heavy ion beams. The ion beams, each with a final focus radius $r_{bf} \geq R$ (R is the target radius), are all assumed to irradiate the target at the same angle α_0 and symmetrically with respect to the equatorial plane. Separate one dimensional (1-D) simulations for the pole and equator target sectors indicate that the $\ell = 2$ mode in the asymmetry of fuel implosion vanishes for $\alpha_0 \approx 36°$. The $\ell = 4$ mode can also be eliminated by adjusting the ion current profile across each beam. It is conjectured that the higher asymmetry modes with $\ell \geq 6$ will be smoothed out by radiative symmetrization to $\lesssim 1\%$. A 1-D average (over the target latitude) energy gain of G = 57 is calculated.

1. INTRODUCTION

In the preceding paper (hereafter referred to as Paper I) a new version of indirect drive target for heavy ion inertial fusion (HIIF) is proposed. In this target the fusion capsule is centred inside the *hotraum* — a spherical cavity filled with deuterium at a near solid density and surrounded by a high Z casing. When heated to the 'working' temperature of $T \simeq 100$–300 eV, the hotraum becomes virtually transparent for photons with $h\nu \gtrsim 300$ eV and allows effective radiative symmetrization of the ablative drive on the fusion capsule. At the same time, the hotraum cavity contains enough material to absorb a significant portion of the initial ion energy; hence, all the non-uniformities of the ion energy deposition and the range variations due to the heating and expansion of the absorber are confined to the outer region of the hotraum. In contrast to the *hohlraum* targets that have been discussed recently within the context of the indirect drive approach to HIIF [1–5], the hotraum target contains no compact converters; the beam-to-radiation energy conversion takes place directly in the casing and in the adjacent hotraum layer.

The initial configuration of the hotraum target, described in Section 2, is perfectly spherical and requires no special orientation in space; but the target is supposed to work when irradiated by a realistic non-spherical array of heavy ion beams. Paper I dealt exclusively with the physical aspects of the hotraum performance and relied on one dimensional (1-D) hydrodynamics simulations carried out under the simplifying assumption of *spherically symmetric* irradiation by ions moving strictly along radial directions. In the present paper, this assumption is relaxed and the target performance is analysed for a specific *non-spherical* two dimensional (2-D) arrangement of irradiating ion beams (described in Section 3) that may be easier to realize than the spherical one.

Of course, a proper investigation of our target under the conditions of 2-D drive should be conducted with a 2-D hydrodynamics code which includes an adequate model for the radiative energy transport in the hotraum. However, when no such code is available and because 2-D simulations with radiative energy transport are costly anyway, it would be quite expedient to begin with a simpler analysis by exploring the 2-D pattern of energy deposition in the static case and by performing separate 1-D hydrodynamics simulations for different target sectors. Clearly, the possibilities of such an approach are limited and the main question of whether the target will ignite cannot be answered decisively. Nevertheless, one can significantly narrow the range of parameters where ignition is possible, clarify certain 2-D aspects of the target performance and, given a proper insight into the target physics, obtain valuable clues as to what might be expected in 2-D simulations.

* *Permanent affiliation:* Institute of Theoretical and Experimental Physics, B. Cheremushkinskaja 25, Moscow, Russia.

The analysis presented in this paper consists of two distinct parts. Intuitively, it is clear that a good performance of an initially spherical target can be expected only when the incident energy flux of irradiating ions is distributed uniformly enough over the target surface. In Section 4, we solve the relatively simple geometrical problem of finding the beam configuration that provides the most uniform illumination of the target sphere.

However, even a perfectly spherical distribution of the incident energy flux can lead to a non-spherical fuel implosion because ions enter the target surface obliquely, at different angles for different target latitudes. As a result, for a given energy flux on the surface we calculate quite different distributions of the specific deposition power over the radial depth along different radii. In Sections 5 and 6 we take this effect into account and address specifically the problem of implosion symmetry. For this, the results obtained in Section 4 can serve only as a good first guess. By performing separate 1-D hydrodynamics runs for the polar and equatorial target sectors, we show conclusively that the $\ell = 2$ mode in the asymmetry of implosion can be eliminated by choosing the illumination angle to be $\alpha_0 \approx 36°$, which is very close to the angle of the most uniform illumination, $\alpha_0 = 35°16'$, calculated in Section 4. Less definitive is the conclusion that the $\ell = 4$ mode can be eliminated as well by the proper adjustment of the beam current profile. We estimate tentatively that the $\ell = 6$ and higher asymmetry modes of the implosion will be reduced to $\lesssim 1\%$ by the radiative energy redistribution in the hotraum cavity. The target energy gain that is obtained in our 1-D simulations is G = 57.

2. TARGET STRUCTURE AND ION PULSE PARAMETERS

A sectorial view of the initially spherical target configuration is shown in Fig. 1. A detailed discussion of the assumptions and criteria used to select this particular structure and these parameters for the hotraum target is given in Paper I. Except for the thickness of the gold casing, the configuration shown in Fig. 1 coincides with case 2 described in Section 4.3 of Paper I. Here, under the conditions of non-spherical illumination, we had to reduce the casing thickness to 35 μm, as compared with 45 μm in Paper I, in order to let the 6 GeV ^{209}Bi ions pass through the casing and reach the hotraum (at least initially) over the entire casing–hotraum interface, including the target latitudes where

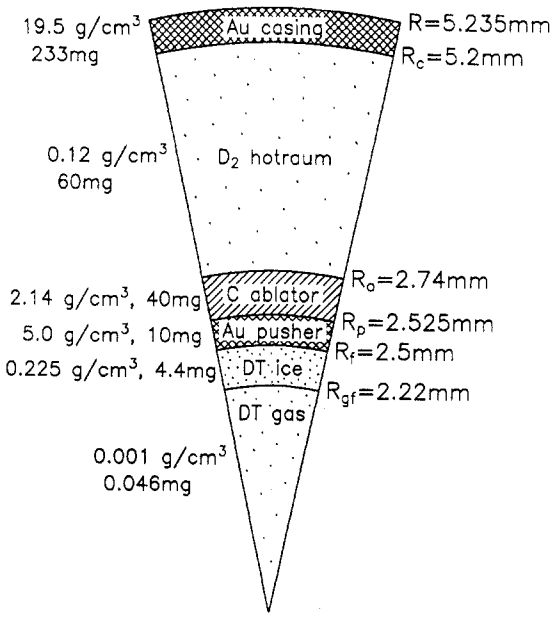

FIG. 1. Sectorial view and initial parameters of the hotraum target investigated in this paper.

all the ion trajectories enter the casing surface obliquely.

We assume that the target is driven by 6 GeV ^{209}Bi ions with the two hump step like power profile shown in Fig. 7 of Paper I. The initial prepulse with power $W_{d1} = 1000$ TW lasts until $t_{d1} = 4$ ns; between t_{d1} and $t_{d2} = 8.5$ ns the pulse power is lowered to $W_{d2} = 300$ TW; after t_{d2} comes the main pulse with $W_{d3} = 1000$ TW which ends at $t_{d3} = 15$ ns. The total input energy

$$E_d = W_{d1}t_{d1} + W_{d2}(t_{d2} - t_{d1}) + W_{d3}(t_{d3} - t_{d2})$$

is equal to 11.85 MJ. These pulse parameters are somewhat different from those used in case 2 of Paper I.

All the target simulations discussed below have been performed with the 1-D three temperature (3-T) hydrodynamics code DEIRA. A brief description of this code is given in Paper I.

3. ILLUMINATION SCHEME

The best illumination scheme for a spherical target would be a perfectly spherical distribution of incoming beams. Such a scheme, however, is regarded as unfeasible for heavy ion beams because of the difficulties associated with turning the beams into the vertical direction. As a

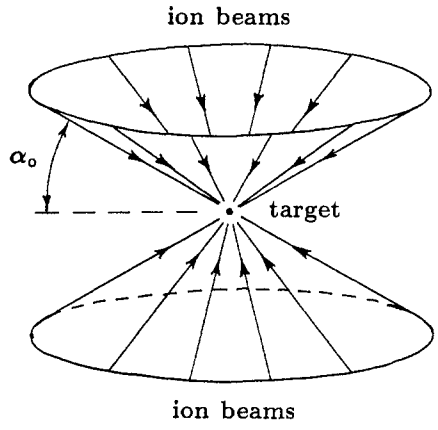

FIG. 2. Illumination scheme: ion beams, arranged in an axially symmetric pattern, all irradiate the target at the same angle α_0 and symmetrically with respect to the equatorial plane.

possible alternative, we consider a simple non-spherical illumination pattern, in which ion beams with final focus $r_{bf} \geq R$ (R is the initial target radius) are incident on the target along a conical surface at an angle α_0 with respect to the equatorial plane (see Fig. 2). Since axial symmetry of illumination does not seem to be much of a problem for the accelerator technique and could be ensured by some 10–40 beams spread uniformly over the azimuth, we assume for simplicity that the beam configuration is perfectly axially symmetric, and symmetric also with respect to the equatorial plane. Under such conditions only even Legendre mode $\ell = 2, 4, 6, \ldots$ of the illumination asymmetries are to be considered.

Let $\rho_b(\vec{\Omega}_b)d\vec{\Omega}_b/4\pi$ be the number fraction of ion beams coming along direction $\vec{\Omega}_b$ (see Fig. 3) within the solid angle $d\vec{\Omega}_b$. The beam distribution function is normalized by the condition

$$\frac{1}{4\pi}\int_{4\pi}\rho_b d\vec{\Omega}_b = \frac{1}{2}\int_{-1}^{+1}\rho_b(\mu_b)d\mu_b = 1 \qquad (1)$$

where $\mu_b = \cos\theta_b$ and θ_b is the polar angle for the direction of incidence of a given beam. For spherical illumination $\rho_b = 1$, while for the 'conical' pattern shown in Fig. 2

$$\rho_b(\mu_b) = \delta(\mu_b - \mu_0) + \delta(\mu_b + \mu_0) \qquad (2)$$

where $\mu_0 = \cos\theta_0 = \sin\alpha_0$ and $\delta(x)$ is the Dirac δ function.

To complete the description of the illumination scheme, we have to postulate a certain distribution of the ion current density within each beam. Assume that, in the vicinity of the target:

(a) each ion beam has a cylindrical shape,
(b) the ion current density is symmetric with respect to the beam axis,
(c) the axis of each beam passes exactly through the target centre.

Let the ion current density at a distance r from the beam axis be proportional to a function $\sigma_b(\xi)$, where $\xi = r/R$ (R is the initial target radius). The function $\sigma_b(\xi)$ is supposed to be normalized by the condition

$$2\int_0^1 \sigma_b(\xi)\xi\, d\xi = 1 \qquad (3)$$

The latter implies that we discard ion trajectories with $\xi > 1$ that miss (at least initially) the target: these ions are simply excluded from the overall energy balance. In what follows, $\sigma_b(\xi)$ is approximated by a one parameter family of inverted parabolas,

$$\sigma_b(\xi) = 1 + \beta_0 - 2\beta_0\xi^2 \qquad (4)$$

which automatically satisfy the normalization condition (3). Physically reasonable values of parameter β_0 lie within the interval $0 < \beta_0 < 1$.

Thus, the illumination scheme considered here is characterized by two free parameters α_0 and β_0. Below, these parameters are used to suppress the $\ell = 2$ and $\ell = 4$ modes in the asymmetry of the DT fuel implosion.

4. UNIFORMITY OF THE ION ENERGY FLUX ON THE TARGET SURFACE

As a first step, consider the distribution of the incident energy flux over the initial target surface. Let P

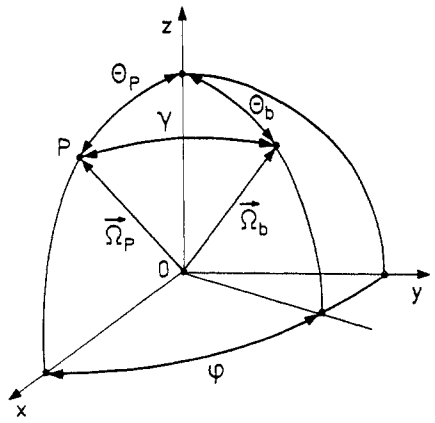

FIG. 3. Spherical co-ordinate notation used throughout the paper: $\vec{\Omega}_P$ is the unit vector along the radial direction towards the point of observation P and $\vec{\Omega}_b$ is the unit vector in the direction of an incident ion beam.

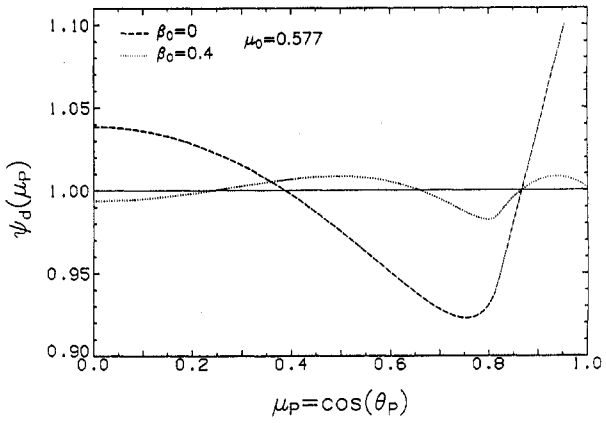

FIG. 4. Angular distribution of the normalized energy flux on the target surface for two values of the parameter β_0 characterizing the ion current distribution across individual beams (see Eq. (4)). The illumination angle $\alpha_0 = \sin^{-1}\mu_0$ is set equal to 35°16', for which there is no contribution from the $\ell = 2$ mode.

be a point of observation upon the target sphere of radius R. Then, the incident energy flux at this point can be calculated as

$$S_d(\vec{\Omega}_P) = \frac{W_d}{\pi R^2}\int_{2\pi}\cos\gamma\,\sigma_b(\sin\gamma)\,\rho_b(\vec{\Omega}_b)\,\frac{d\vec{\Omega}_b}{4\pi}$$

$$\stackrel{\text{def}}{=} \frac{W_d}{4\pi R^2}\,\psi_d(\mu_P) \tag{5}$$

Here W_d is the total power of all incoming beams (the driver power), $\cos\gamma = \vec{\Omega}_P\cdot\vec{\Omega}_b$ (see Fig. 3), $\vec{\Omega}_P$ is the unit vector in the direction of point P, $\vec{\Omega}_b$ is the unit vector in the direction of an incident beam, θ_P and θ_b are the polar angles of vectors $\vec{\Omega}_P$ and $\vec{\Omega}_b$, respectively, and $\mu_P = \cos\theta_P$.

The second part of Eq. (5) defines a dimensionless function $\psi_d(\mu_P)$ that may serve as a measure of uniformity of the ion energy flux on the target surface: for a perfectly uniform flux $\psi_d(\mu_P) = 1$. For the beam distribution given by Eq. (2) we obtain

$$\psi_d(\mu_P) = \frac{2}{\pi}\int_{\mu_1}^{\mu_2}\frac{\sigma_b(\sqrt{1-x^2})x\,dx}{[(1-\mu_P^2)(1-x^2)-(x\mu_P-\mu_0)^2]^{1/2}} + \frac{2}{\pi}\int_{\mu_3}^{\mu_4}\frac{\sigma_b(\sqrt{1-x^2})x\,dx}{[(1-\mu_P^2)(1-x^2)-(x\mu_P+\mu_0)^2]^{1/2}} \tag{6}$$

where

$$\mu_1 = \max\{0;\ \mu_0\mu_P - [(1-\mu_0^2)(1-\mu_P^2)]^{1/2}\} \tag{7a}$$

$$\mu_2 = \mu_0\mu_P + [(1-\mu_0^2)(1-\mu_P^2)]^{1/2} \tag{7b}$$

$$\mu_3 = 0 \tag{7c}$$

$$\mu_4 = \max\{0;\ -\mu_0\mu_P + [(1-\mu_0^2)(1-\mu_P^2)]^{1/2}\} \tag{7d}$$

In particular, at the equator and poles we have

$$\psi_d(0) = \frac{4}{\pi}\int_0^{\sqrt{1-\mu_0^2}}\sigma_b(\sqrt{x^2+\mu_0^2})\,dx \tag{8}$$

$$\psi_d(1) = 2\mu_0\sigma_b(\sqrt{1-\mu_0^2}) \tag{9}$$

For the illumination pattern described in Section 3, the distribution of the incident flux $\psi_d(\mu_P)$ is a function of two free parameters $\mu_0 = \sin\alpha_0$ and β_0. The most uniform (in the sense that it contains only the $\ell = 6$ and higher Legendre harmonics) profile of $\psi_d(\mu_P)$ is obtained for $\mu_0 = 0.577$ and $\beta_0 = 0.40$; it is shown as a dotted curve in Fig. 4. To illustrate how $\psi_d(\mu_P)$ looks for a different ion current distribution, a plot of ψ_d for $\mu_0 = 0.577$ and $\beta_0 = 0$ (dashed curve) is also given. From Fig. 4 one learns that the peak-to-valley fluctuations in the incident energy flux can be reduced to 2.5%; the corresponding RMS deviation is 0.7%.

More detailed information about the angular scale of non-uniformities in the incident flux can be obtained from the expansion into Legendre polynomials

$$\psi_d(\mu_P) = 1 + \sum_{k=1}^{\infty} c_{2k}P_{2k}(\mu_P) \tag{10}$$

where

$$c_\ell = (2\ell+1)\int_0^1\psi_d(\mu_P)P_\ell(\mu_P)\,d\mu_P \tag{11}$$

The dependences of the first three ($\ell = 2$, 4 and 6) amplitudes c_ℓ on μ_0 are plotted in Fig. 5 for two

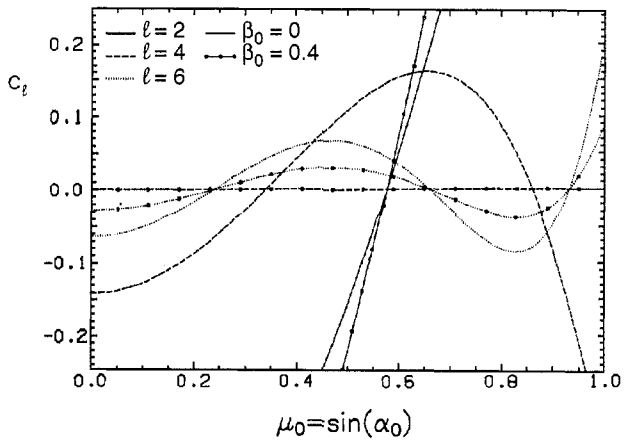

FIG. 5. Amplitudes of the three lowest Legendre modes in the asymmetry of the energy flux on the target surface plotted versus the sine of the illumination angle α_0. The three curves (solid, dashed and dotted) marked with black dots correspond to $\beta_0 = 0.4$, for which the $\ell = 4$ mode vanishes. The three curves without dots correspond to $\beta_0 = 0$.

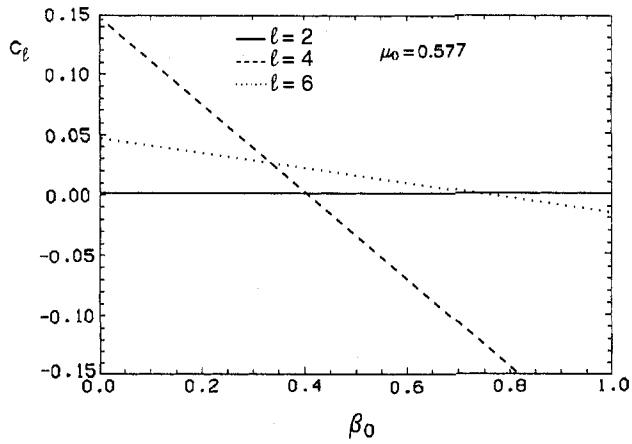

FIG. 6. Same asymmetry mode amplitudes as in Fig. 5 plotted versus the parameter β_0 characterizing the ion current profile (see Eq. (4)). The illumination angle α_0 is set equal to 35°16', for which the $\ell = 2$ mode vanishes.

values of β_0. A remarkable fact is that, independent of the ion current profile $\sigma_b(\xi)$, the second harmonic c_2 always vanishes at $\mu_0 = 1/\sqrt{3} = 0.577$ ($\alpha_0 = \sin^{-1} 1/\sqrt{3} = 35°16'$), which is just the zero of the second Legendre polynomial $P_2(\mu_0) = \frac{1}{2}(3\mu_0^2 - 1)$. To prove this fact analytically, it is sufficient to substitute

$$\sigma_b(\xi) = \frac{1}{2\xi_0}\,\delta(\xi - \xi_0)$$

into Eqs (6) and (11), and verify by straightforward integration that c_2 vanishes at $\mu_0 = 1/\sqrt{3}$ for arbitrary ξ_0. Since ψ_d depends linearly on σ_b, the latter implies that c_2 vanishes at $\mu_0 = 1/\sqrt{3}$ for arbitrary $\sigma_b(\xi)$. A similar result was obtained earlier by Buchwald et al. [6] who considered the same illumination scheme, but for a Gaussian profile of the ion current density. By performing a numerical integration, they were capable of calculating the optimal illumination angle only approximately and obtained $\alpha_0 \approx 33°$. From Fig. 5 one sees that c_2 is a rather steep function of μ_0: to keep the amplitude of the $\ell = 2$ harmonic below, say, 2%, the value of α_0 must be set with an accuracy of better than 1°.

Figure 6 shows that, by choosing $\beta_0 = 0.40$, the fourth harmonic $\ell = 4$ can also be eliminated. The remaining asymmetries in the sixth and higher harmonics add up to 2.5% of the peak-to-valley variation in the energy flux $S_d(\mu_P)$ (see Fig. 4). Since c_2 vanishes at $\alpha_0 = 35°16'$ independently of β_0, we can say that the illumination angle α_0 controls the amplitude of the $\ell = 2$ mode, while the ion current distribution in individual beams determines the amplitude of the $\ell = 4$ harmonic of the non-uniformities in the energy flux on the target surface.

5. TWO DIMENSIONAL MODEL FOR THE ION ENERGY DEPOSITION

Even if the non-uniformity of the energy flux on the target surface is small and can be neglected, the ion penetration front still lies at different radial depths for different target latitudes (see Fig. 7). For $\mu_0 = 0.577$, the ratio between the penetration depths into a thin uniform absorber at $\mu_P = 1$ (pole) and $\mu_P = \mu_0$ is 0.577:1. Hence, despite a mere 2.5% asymmetry in the incident energy flux obtained for $\mu_0 = 0.577$ and $\beta_0 = 0.4$, there still remain significant non-uniformities in the distribution of the specific power of ion energy deposition. To describe them quantitatively, the following model is employed.

Let $\vec{\Omega}_P$ be a unit vector in the direction of a radial ray along which the energy deposition rate $q_d(\vec{r})$ (TW/mg) is to be calculated as a function of spherical radius $r = |\vec{r}| = |r\vec{\Omega}_P|$ (see Fig. 3). If we assume now that the penetration depth of the beam ions is small compared with the target radius R, we can introduce a local planar approximation to the spherical geometry of the absorbing layer in the vicinity of the entrance point $\vec{r} = R\vec{\Omega}_P$. In this approximation we obtain

$$q_d(\vec{r}) = \frac{W_d}{\pi r^2 \epsilon_{b0}} \int_{2\pi} \cos\gamma\, \sigma_b(\sin\gamma)\rho_b(\vec{\Omega}_b) \times \frac{\partial \epsilon_{bi}(\vec{r}, \vec{\Omega}_b)}{\rho \partial r} \frac{d\vec{\Omega}_b}{4\pi} \qquad (12)$$

where $\epsilon_{bi} = \epsilon_{bi}(\vec{r}, \vec{\Omega}_b)$ is the energy of individual ions, incident upon the target surface along $\vec{\Omega}_b$ (at the angle

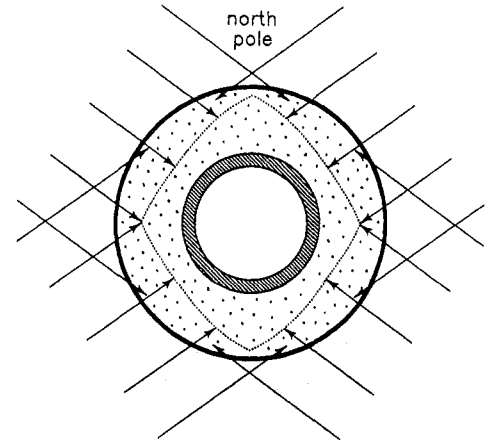

FIG. 7. Penetration front (dotted line) of 6 GeV ^{209}Bi ions into the target depicted in Fig. 1. The illumination parameters are $\mu_0 = 0.577$ and $\beta_0 = 0.4$, corresponding to the most uniform distribution of the ion energy flux on the target surface.

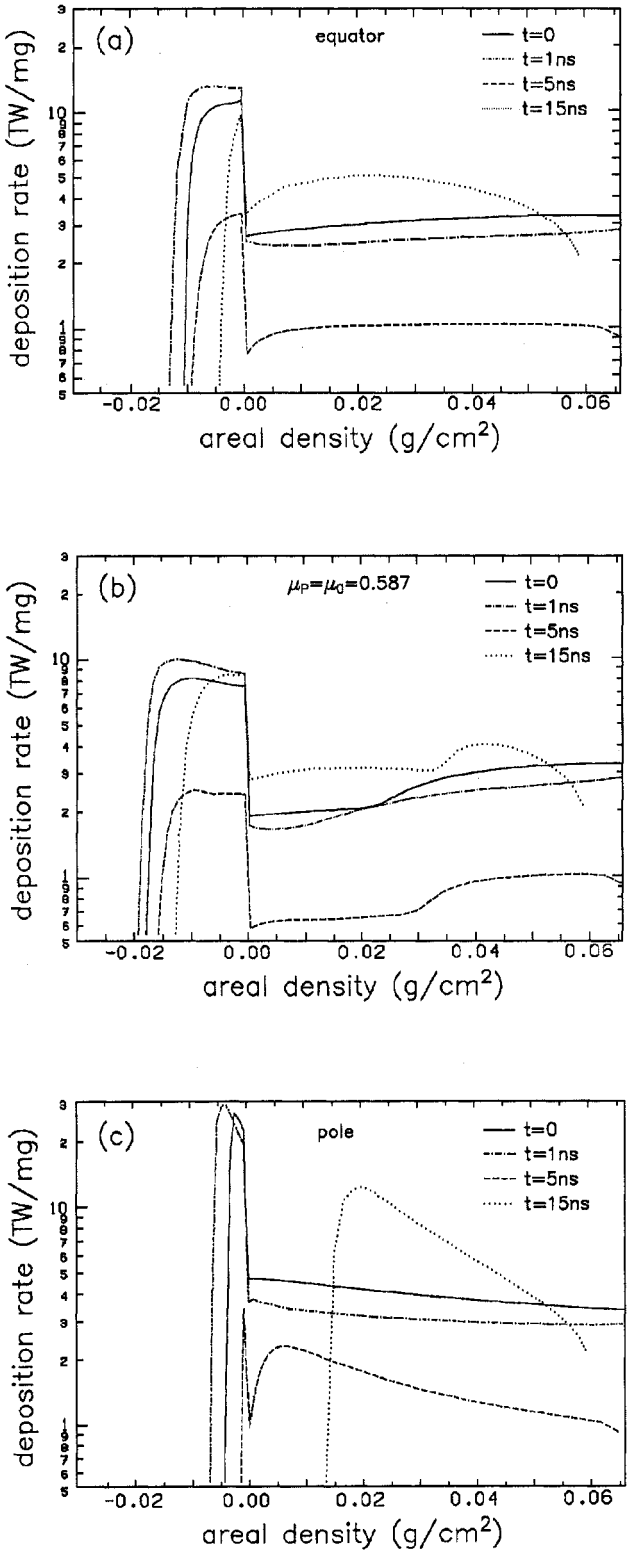

FIG. 8. Profiles of the specific ion deposition power along (a) the equator ($\mu_P = 0$), (b) the mid-latitude ($\mu_P = \mu_0 = 0.587$) and (c) the pole ($\mu_P = 1$) target radii at four characteristic times during the ion pulse. Zero areal density is assigned to the casing–hotraum interface with initial radius $R_c = 5.2$ mm.

γ with respect to $\vec{\Omega}_P$), as measured at point $\vec{r}$; $\epsilon_{b0} = 6$ GeV is the initial value of the ion energy; all the other notation is the same as that in Eq. (5). To calculate $\epsilon_{bi}(\vec{r}, \vec{\Omega}_b)$ for given $\vec{\Omega}_P$ and $\vec{\Omega}_b$, one has to solve the stopping equation

$$\frac{\partial \epsilon_{bi}(\vec{r}, \vec{\Omega}_b)}{\partial r} = \frac{\rho}{\cos\gamma} S_{bi}(\vec{r}, \epsilon_{bi}) \qquad (13)$$

with the boundary condition $\epsilon_{bi}(R\vec{\Omega}_P, \vec{\Omega}_b) = \epsilon_{b0}$; here the stopping power S_{bi} is determined by the local plasma conditions and the value of the ion energy ϵ_{bi} at $\vec{r}$. In the target simulations discussed below, the full scale model of ion stopping in plasmas from Ref. [7] was used to calculate S_{bi}.

The structure of the right hand side of Eq. (12) is similar to that of Eq. (5). The only difference is that R^2 in the denominator before the integral in Eq. (5) is replaced by r^2 in Eq. (12). This is required to preserve the energy balance when Eq. (12) is used in a spherical geometry: integrating the right hand side of Eq. (12) over the entire absorber mass, we recover the total driving power W_d. For $\rho_b(\vec{\Omega}_b)$ given by Eq. (2), the integral in Eq. (12) reduces to the same form as that in Eq. (6).

The variation of the ion penetration depth over the target latitude, as calculated with the above model, is shown in Fig. 7. The two illumination parameters are fixed at their 'best' values, $\mu_0 = 0.577$, $\beta_0 = 0.4$, corresponding to the minimum (2.5% peak-to-valley variation) non-uniformity of the energy flux on the target surface. It is clearly seen that the penetration depth fluctuates with a considerably larger amplitude, and these fluctuations occur on an angular scale corresponding mainly to the $\ell = 2$ and $\ell = 4$ harmonics. The ion energy deposition profiles at three characteristic latitudes are shown in Fig. 8.

6. SYMMETRY OF IMPLOSION

In Paper I it is shown that even if the hydrodynamic perturbations from the ion deposition region do reach the fuel, it happens so late that they cannot destroy the symmetry of the fuel implosion. Under such conditions the fusion capsule is virtually decoupled hydrodynamically from the deposition region and the symmetry of its implosion is controlled:

(a) by the accuracy of fabrication,
(b) by the uniformity of the radiative energy flux entering the capsule (we assume that the capsule is designed in such a way that it does not fail to ignite due to the Rayleigh–Taylor instability).

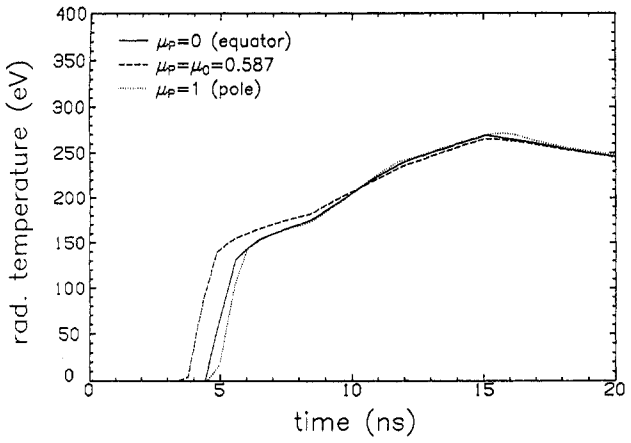

FIG. 9. Temporal behaviour of the radiation temperature at the surface of the fusion capsule.

In what follows we analyse the 2-D aspects of implosion by performing separate 1-D simulations for different target sectors. With this approach no transverse (with respect to the radial direction) energy transport is allowed in the hotraum. Hence, we can expect that the 2-D simulations where this transport is accounted for will always demonstrate a better implosion symmetry (for a perfectly fabricated capsule) than the separate 1-D runs — but perhaps for slightly different values of the free parameters in the illumination scheme. Also, the real values of the radiation smoothing factor should be higher than those calculated in Refs [8–10] under the approximation of a single photon pass in a cavity between two spheres.

Figure 7 shows that the ion penetration depth changes from an absolute minimum at $\mu_P = 1$ (pole) to an absolute maximum at $\mu_P = \mu_0$ (mid-latitude) and back to a local minimum at $\mu_P = 0$ (equator). Accordingly, we look for values of the two illumination parameters, μ_0 and β_0, which ensure perfect synchronization of the fuel implosion in the three 1-D runs corresponding to these three latitudes. It is quite clear that the pole and equator runs can always be synchronized by choosing an appropriate value of μ_0. Less trivial is the fact that all three runs can be synchronized with β_0 confined to the interval $0 < \beta_0 < 1$. Nevertheless, the calculations show that this is the case (at least for the target studied here) and a practically perfect synchronization is obtained for $\mu_0 = 0.587$, $\beta_0 = 0.06$. The latter value of μ_0 is quite close to 0.577, for which the second Legendre harmonic in the asymmetry of the energy flux vanishes. A considerable difference between the two values of $\beta_0 = 0.06$ and $\beta_0 = 0.4$, obtained respectively for synchronized implosion and when eliminating the $\ell = 4$ harmonic in the energy flux distribution, indicates a strong presence of the $\ell = 4$ asymmetry mode in the illumination scheme under discussion.

Figures 8–10 and Table I provide detailed information on the target performance in the three synchronized 1-D runs. Figure 8 illustrates the asymmetry of the ion energy deposition at different phases of the ion pulse. In Fig. 8(c) one sees that after $t \simeq 5$ ns the ions do not actually reach the hotraum in the vicinity of the target pole and liberate all their energy inside the gold casing — in sharp contrast with the mid-latitude run shown in Fig. 8(b). Note also that, unlike the best uniform distribution of the energy flux discussed in Section 4, the total deposition energy E_{dep} (per steradian) varies now by some 20% over the target latitude.

Figure 9 shows that the equatorial and polar target sectors have almost identical time histories of radiation temperature on the ablator surface of the fusion capsule. At mid-latitude, the radiation pulse arrives about 1 ns earlier than at the pole; however, this difference (occurring on the angular scale corresponding to the $\ell = 4$ mode) should be reduced by a factor of about 2–4 when the transverse energy transport and multi-frequency effects discussed in Paper I are properly accounted for.

The general r–t diagram of the target performance is similar to those shown in Figs 3 and 10 of Paper I. Here, to give a conspicuous view of the implosion symmetry, an enlargement of the r–t diagram near the time of stagnation for two characteristic Lagrangian elements of the DT fuel is shown in Fig. 10. One

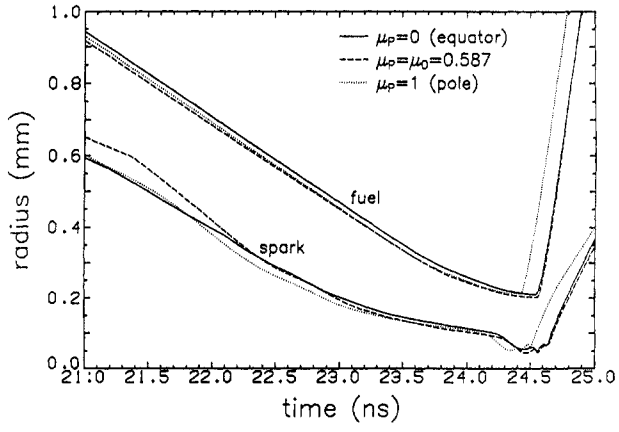

FIG. 10. Radius–time diagrams of the fuel–pusher interface (the 'fuel' curves) and of the initial interface between the DT gas and the solid (the 'spark' curves) along the equator, mid-latitude and pole target radii. The Lagrangian position of the thermonuclear spark boundary practically coincides with that of the interface between the DT gas and the solid.

TABLE I. RESULTS OF SIMULATIONS FOR THREE DIFFERENT SECTORS OF THE SYNCHRONIZED HOTRAUM TARGET

Energy partition (MJ/sr)	Equator	Mid-latitude	Pole	Paper I[a]
E_{dep}	$12.0/4\pi$	$11.28/4\pi$	$13.65/4\pi$	$10/4\pi$
$E_{dep,h}$	$2.39/4\pi$	$3.40/4\pi$	$1.16/4\pi$	$4.33/4\pi$
E_{c-h}	$1.54/4\pi$	$0.53/4\pi$	$2.59/4\pi$	$-0.06/4\pi$
E_{loss}	$3.07/4\pi$	$2.54/4\pi$	$4.42/4\pi$	$0.53/4\pi$
E_{caps}	$1.59/4\pi$	$1.57/4\pi$	$1.60/4\pi$	$1.61/4\pi$
E_{pusher}	$0.052/4\pi$	$0.046/4\pi$	$0.081/4\pi$	$0.048/4\pi$
E_{fuel}	$0.45/4\pi$	$0.43/4\pi$	$0.46/4\pi$	$0.44/4\pi$
Ignition parameters				
t (ns)	24.499	24.514	24.394	24.333
R_{DT} (mm)	0.212	0.203	0.212	0.208
$\langle\rho r\rangle_{DT}$ (g/cm^2)	2.35	2.73	2.47	3.1
E_{fusion} (MJ/sr)	$677/4\pi$	$683/4\pi$	$696/4\pi$	$757/4\pi$
Burn fraction	0.45	0.45	0.46	0.46
Gain	56.4	60.5	51.0	75.7

[a] Results from Paper I (case 2 in Tables I and III) obtained with the approximation of radial beam propagation and perfectly spherical illumination.

clearly sees that the asymmetry of the pusher-fuel interface near stagnation does not exceed a few per cent. The spark boundary, which in Lagrangian co-ordinates practically coincides with the initial interface between the DT gas and ice, manifests higher relative distortions, especially in about the last 0.2 ns before the ignition. From Fig. 10 one can infer that, to keep the $\ell = 2$ asymmetry of the outer fuel boundary within tolerable limits, the polar and equatorial stagnation times must be synchronized to $\Delta t \lesssim 0.4$ ns. Deformation of the central spark region is more sensitive to the drive asymmetries and may require a synchronization down to $\Delta t \lesssim 0.1$–0.2 ns. When expressed in terms of the accuracy limits for the illumination angle α_0, such synchronization requirements imply $\alpha_0 = 35°54' \pm 0°07'$ for $\Delta t \simeq 0.4$ ns and $\alpha_0 = 35°54' \pm 0°02'$ for $\Delta t \simeq 0.1$ ns. The constraints on the second illumination parameter β_0 are expected to be less stringent because of the more effective radiative smoothing of the $\ell = 4$ mode.

In Table I various energy characteristics and ignition parameters of the three synchronized 1-D runs are listed. One sees that the energy deposited directly in the hotraum, $E_{dep,h}$, varies strongly with the target latitude. These variations, however, are almost fully compensated for by the radiative energy transfer from the casing into the hotraum, E_{c-h}: the sum $E_{dep,h} + E_{c-h}$ remains constant to within 5%. As a consequence, only a small variation of about 2% is observed for the energy E_{caps} that enters the fusion capsule.

All the three simulation runs discussed here exhibit significantly higher values of the radiative energy loss, E_{loss}, from the outer target surface than that from the same target driven by radially propagating ions in case 2 of Paper I. The reason is that a large fraction of irradiating ions enter the target surface obliquely. As a result, the target casing is heated more intensely than in the case of radial ion trajectories and the radiative losses reach 25–30% of the total energy input. The thermonuclear energy gain falls by almost the same amount in comparison with the one calculated in Paper I. Such high radiative losses calculated for the ion energy $\epsilon_{bi} = 6$ GeV suggest that probably the same or even higher target efficiency can be obtained with somewhat higher values of the ion energy, $\epsilon_{bi} \approx 7$–8 GeV.

With the illumination parameters μ_0 and β_0 adjusted to synchronize the capsule implosion along the $\mu_P = 0$, $\mu_P = \mu_0$ and $\mu_P = 1$ radial directions, we can go one step further and calculate the full angular distribution of the energy E_{caps} that enters the fusion capsule at different target latitudes. Figure 11 shows the values

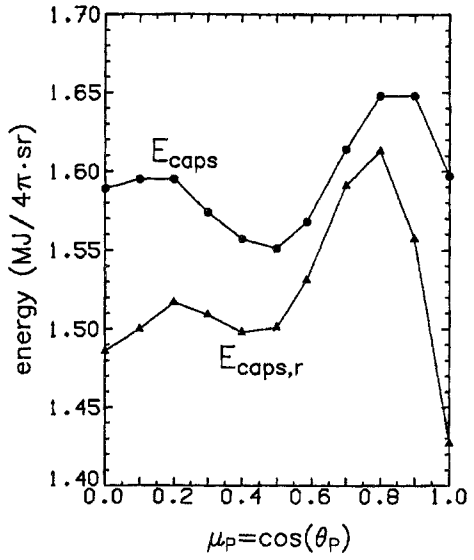

FIG. 11. Total (radiation plus work PdV) energy, E_{caps}, and radiation energy, $E_{caps,r}$, entering the fusion capsule across the ablator–hotraum interface along 11 different target radii as calculated in 11 separate 1-D hydrodynamics runs.

of E_{caps} (filled circles) at 11 equally spaced values of μ_P as calculated in 11 separate 1-D runs. It is clearly seen that E_{caps} varies on the angular scale corresponding to the $\ell = 6$ harmonic; the peak-to-valley amplitude of this variation is $\Delta E_{caps}/E_{caps} = 6\%$. Although the total energy transfer E_{caps} through the ablator–hotraum interface is dominated by radiation, a certain fraction is also contributed by mechanical work. The radiative component $E_{caps,r}$ of E_{caps}, shown in Fig. 11 with filled triangles, exhibits the same angular dependence as E_{caps} but with twice as high an amplitude, $\Delta E_{caps,r}/E_{caps,r} = 12\%$. This is a clear manifestation of the damping effect of the mechanical interaction between the ablated capsule material and the hotraum fill: a higher radiation flux into the capsule leads to a more intensive ablative expansion, which, in its turn, reduces the work PdV done by the hotraum gas against the capsule ablator.

In reality, the angular variations of E_{caps} and $E_{caps,r}$ shown in Fig. 11 will be smoothed by the transverse radiative energy transport across the hotraum. The highest smoothing factors are expected for the smallest angular scales. Although the physical situation is simplified by the fact that the fusion capsule is hydrodynamically decoupled from the absorber (see Section 4.5 of Paper I) and no non-linear effects are expected from the transverse pressure gradients in the heated region, only full scale 2-D simulations can establish reliably the level of residual asymmetries in the ablative capsule drive. Nevertheless, if we make use of the radiative symmetrization calculations performed in Refs [8–10], we can make the following tentative estimate. The authors of Refs [8–10] assumed that the inner casing surface at $r = r_{em} = R_c$ emitted photons with a non-uniform brightness distribution and calculated the reduction factor $f_{red}(\ell, x)$ for the non-uniformity of illumination of the capsule surface at $r = R_a < r_{em}$ as a function of the Legendre mode number ℓ and the cavity radii ratio $x = R_a/R_c$. For $x = 0.5$ and $\ell = 6$, a value $f_{red} = 20$ is quoted in Ref. [9]. One might argue that in our case, where a substantial fraction of the primary radiation is emitted by the hotraum gas at $3.7 < r_{em} < 5.2$ mm $= R_c$ and the ratio $x = R_a/r_{em}$ ranges from 0.5 to 0.75, the effective reduction factor must be significantly lower than that calculated for $x = 0.5$. Notice, however, that only a small fraction, ranging from 7 to 16%, of the primary radiation emitted at $3.7 < r_{em} < 5.2$ mm falls directly on the ablator surface with $R_a = 2.74$ mm. The remaining part of this radiation is absorbed and re-emitted several times by the gold casing, before eventually about 50% of the initially emitted energy enters the central capsule [9, 1]. The symmetrization factor for the re-emitted radiation is higher than that calculated in Refs [8–10]. As a net result of all these effects, we conjecture a reduction factor of $f_{red} \approx 10$ for the $\ell = 6$ mode in our target. The latter means that in reality we can expect the peak-to-valley variations of E_{caps} to be $\lesssim 1\%$. The amplitudes of $\ell = 8$ and higher harmonics will be even smaller because, on the one hand, their initial contribution decays rapidly with increasing ℓ owing to a large beam focal spot, $r_{bf} \geq R$, and, on the other hand, the symmetrization factors increase with ℓ. The $\lesssim 1\%$ peak-to-valley variation of the driving energy flux upon the fusion capsule meets well the constraints on the pressure non-uniformities deduced from the 2-D hydrodynamics simulations [11, 12].

7. CONCLUSIONS

The hotraum target was conceived as a possible means of achieving a spherical implosion of the fusion capsule in a target driven by a realistic non-spherical arrangement of heavy ion beams. An important restriction imposed on the target design is that its initial configuration should be spherically symmetric and require no special orientation in the reactor chamber. The smoothing of illumination asymmetries occurs via radiative energy transport in the hotraum — a cavity

filled with a low Z low density material which is transparent to thermal X rays and opaque to the incoming beam ions. For efficient smoothing, it is advantageous to allot a large volume to the hotraum cavity. However, the target efficiency rapidly deteriorates with the increasing hotraum volume. As a reasonable compromise, the following strategy has been adopted:

(a) A moderate value of $R_a/R_c = 0.5$ is assumed for the hotraum radial proportion which, on the one hand, ensures low amplitudes of high order asymmetry modes with $\ell \geq 6$ and, on the other hand, still allows high enough target gains of $G \gtrsim 50$.

(b) All odd ($\ell = 1, 3, 5, \ldots$) asymmetry modes and the lowest even ($\ell = 2$) asymmetry mode are supposed to be eliminated by the proper arrangement of the geometric pattern of the irradiating ion beams.

(c) The freedom still remaining in choosing the parameters of the illumination scheme is used to suppress (at least partially) the intermediate $\ell = 4$ mode. Additional smoothing of this mode can be expected from radiative energy redistribution in the hotraum cavity.

The specific illumination scheme to which these prescriptions have been applied involves an axially symmetric array of cylindrical ion beams all falling upon the target at the same angle α_0 and symmetrically with respect to the equatorial plane. It is parametrized with two variables — the illumination angle α_0 and the parameter β_0 which characterizes the ion current profile in each beam. The problem that can be solved most easily is the minimization of the non-uniformity of the incident energy flux on the target surface: the $\ell = 2$ mode vanishes for $\alpha_0 = \sin^{-1} 1/\sqrt{3} = 35°16'$ independently of the β_0 value; with $\beta_0 = 0.40$, the $\ell = 4$ harmonic is eliminated as well. However, because of the finite range of the beam ions, this solution does not lead to the best symmetry of the fuel implosion.

An adequate analysis of the implosion symmetry requires 2-D hydrodynamics simulations with full account taken of radiative energy transfer. In this paper, use has been made of a simpler approach based on separate 1-D hydrodynamics simulations along different radial directions of the target. The possibilities of this approach are certainly limited and most of the conclusions reached should be interpreted as suggestive rather than definitive. Nevertheless, the main conclusion that the illumination asymmetries can be smoothed out to an acceptable level appears quite encouraging.

Undoubtedly, the most accurate results are obtained for the lowest $\ell = 2$ asymmetry mode. Since neither radiative smoothing [8–10] nor hydrodynamical 'communication' (it takes more than 20 ns for a sound signal to traverse the hotraum from the pole to the equator) are efficient between the polar and equatorial sectors, we expect the $\ell = 2$ asymmetry to be adequately represented by the two 1-D runs along these two directions. In particular, the 2-D simulations will almost certainly confirm that the $\ell = 2$ mode vanishes at $\alpha_0 = 35°54'$ (or at a value very close to this). However, 2-D calculations are necessary to verify that the $\ell = 4$ and $\ell = 6$ asymmetry modes pose no danger for the fuel implosion and to recalculate the target energy gain. In addition, of course, all the effects due to the Rayleigh–Taylor instability should be studied within the framework of 2-D (or even 3-D) hydrodynamics.

Finally, it should be noted that there are a number of factors that would tend to degrade the 1-D energy gains calculated in Paper I and in this work. Among these are the residual asymmetry of the fuel implosion, the Rayleigh–Taylor instability of the carbon–gold interface in the fusion capsule and the inevitable energy losses in the beam fringes that miss the target. On the other hand, the target considered here has not been properly optimized and its performance can, of course, be improved. As already mentioned in Paper I, the target efficiency noticeably improves when the hotraum opacity is increased by a factor of about 3, which can be realized by using, for example, a low density plastic foam soaked with liquid deuterium to fill the hotraum. A proper 2-D study with multifrequency radiation transport may reveal that the required symmetry of implosion can be achieved with a smaller relative hotraum volume, corresponding to $R_a/R_c > 0.5$. By allowing higher values of the fractional capsule radius R_a/R_c, one could significantly enhance the target energy gain. A heterogeneous structure of the hotraum and a better choice of the ablator material might also have certain advantages.

ACKNOWLEDGEMENTS

I greatly appreciate stimulating discussions with S. Atzeni, J. Meyer-ter-Vehn, R. Piriz and C. Rubbia. I am grateful also to J. Meyer-ter-Vehn and S. Witkowski for providing an opportunity to work at the Max-Planck-Institut für Quantenoptik. This work was supported by the Deutsche Bundesministerium für Forschung und Technologie.

REFERENCES

[1] MURAKAMI, M., MEYER-TER-VEHN, J., Nucl. Fusion **31** (1991) 1315.
[2] MURAKAMI, M., MEYER-TER-VEHN, J., Nucl. Fusion **31** (1991) 1333.
[3] MEYER-TER-VEHN, J., MURAKAMI, M., Part. Accel. **37–38** (1992) 519.
[4] TEMPORAL, M., ATZENI, S., Nucl. Fusion **32** (1992) 557.
[5] TAHIR, N.A., ARNOLD, R.C., BLENSKI, T., LIGOU, J., DEUTSCH, C., Nucl. Fusion **32** (1992) 581.
[6] BUCHWALD, G., GRAEBNER, G., THEIS, J., et al., Laser Part. Beams **1** (1983) 335.
[7] BASKO, M.M., Fiz. Plazmy **10** (1984) 1195 (English translation: Sov. J. Plasma Phys. **10** (1984) 689).
[8] MURAKAMI, M., NISHIHARA, K., Jpn. J. Appl. Phys. **25** (1986) 242.
[9] CARUSO, A., in Inertial Confinement Fusion (Proc. Course and Workshop Varenna, 1988), Editrice Compositori, Bologna (1989) 139.
[10] CARUSO, A., STRANGIO, C., Nucl. Fusion **31** (1991) 1399.
[11] McCRORY, R.L., VERDON, C.P., in Inertial Confinement Fusion (Proc. Course and Workshop Varenna, 1988), Editrice Compositori, Bologna (1989) 83.
[12] ATZENI, S., Europhys. Lett. **11** (1990) 639; Laser Part. Beams **9** (1991) 233.

(Manuscript received 24 September 1992
Final manuscript received 1 March 1993)